Interparticle Contact in Drying Polymer Dispersions Probed by Time Resolved Fluorescence

Andrey Turshatov, Jörg Adams, and Diethelm Johannsmann*

Institute of Physical Chemistry, Clausthal University of Technology, Arnold-Sommerfeld-Strasse 4, D-38678 Clausthal-Zellerfeld, Germany

Received March 11, 2008; Revised Manuscript Received May 6, 2008

ABSTRACT: Using time-resolved fluorescence spectroscopy, we have monitored the coalescence of polymer particles during the film formation process. The accessible parameters are the efficiency of fluorescence resonance energy transfer (FRET) between donor-labeled and acceptor-labeled particles, the scattering intensity, and the fluorescence lifetime of the donor in the absence of the acceptor. The FRET efficiency substantially increases during drying, even though the glass temperature of the material is around the drying temperature. This finding evidences polymer interdiffusion across the interparticle boundaries even without high-temperature annealing. Both the FRET efficiency and scattering intensity show a sigmoidal dependence on drying time. The transition times of the two curves coincide for soft materials, whereas they differ for materials with a T_g around the drying temperature. In the latter case, the FRET efficiency—probing interparticle contact—goes through the transition earlier than the scattering intensity and the donor lifetime. Cohesive interparticle contacts form before the end of the compactification stage, thereby reducing the likelihood of crack formation during drying.

Introduction

Films formed from aqueous polymer dispersions find ever-increasing use in industry because the process of application is environmentally friendly.[1–3] Since the material is based on water as the continuous phase, the amount of volatile organic compounds (VOCs) released into the atmosphere is small. Film formation from polymer dispersions is typically described as a three-stage process.[4,5] In stage I ("consolidation") the water evaporates until the particles touch. In stage II ("compactification"), the particles deform, eventually forming polyhedra with all interstitial water removed. At the end of stage II, the film is transparent. Importantly, film formation is not complete at this time. In order to develop mechanical strength, the film must go through stage III ("coalescence"). In the process of coalescence, the surfactant membranes in-between the particles rupture and polymer chains diffuse across the boundaries, thereby inducing cohesion and toughness.[5] Whether or not the interfaces between the particles completely disappear depends on the details.[6] However, some interdiffusion is critical for mechanical integrity, even if a memory of the particulate nature of the starting material is retained in the final film. For coatings formulations (containing polymers with a glass temperature T_g close to room temperature), the interdiffusion stage can last for days or months. Evidently, it can be shortened by high-temperature annealing.

Indirect evidence for interdiffusion is gained from measurements of the fracture energy.[7] When plotting the fracture energy versus the square root of annealing time, one finds a linear relationship for short annealing times. The $t^{1/2}$-scaling suggests that the increase in mechanical strength is brought about by a diffusion processes. Interdiffusion upon high-temperature annealing was also investigated with small-angle neutron scattering (SANS).[8,9] Using SANS in conjunction with deuterium labeling, one can obtain a rather detailed view of the polymer conformation as well as polymer intermixing. In particular, it could be shown that coil expansion can entropically drive the intermixing process, if the particles initially are smaller than the radius of gyration.[10]

* Author for correspondence. E-mail: johannsmann@pc.tu-clausthal.de. Telephone: +49 5323 - 72 3768. Fax: +49 5323 - 72 4835.

Most past studies have been concerned with interdiffusion induced by annealing. However, interparticle cohesion developing *while the film dries* also is of much importance in the context of cracking. Particle deformation implies uniaxial shrinkage and a tensile in-plane stress. The balance of forces at the particle surface is governed by the material's resistance to deformation, on the one hand, and the ability of the interface to sustain tensile stress, on the other. Cracking should therefore be reduced by polymer interdiffusion, if the latter occurs soon after the first contact.

As the Winnik group has pointed out, fluorescence resonance energy transfer (FRET) constitutes a versatile approach to interdiffusion.[11,12] For instance, the group recently reported on interdiffusion of BA/MMA copolymers.[13] They concluded that a high BA content leads to long-chain branching, which can explain the diffusion data as well as the rheological spectra of their samples. In FRET measurements, one employs dye-labeled polymers, where half of the particles carry a fluorescence donor, while the other half carries an acceptor. When donor and acceptor molecules approach each other to a distance close to their Förster radius, energy is directly transferred from the donor to the acceptor. The Förster radius, R_0, typically is of the order of a few nm and FRET therefore is a probe of proximity between donors and acceptors. Energy transfer has a clear experimental signature in the fluorescence spectra and in the decay curves. The efficiency of energy transfer increases substantially when dye labels cross the interparticle boundaries and intermix. If the fluorescent probes are covalently attached to the polymer backbones, FRET probes the motion of entire chains.

For most samples of practical relevance, polymer intermixing is a rather complicated process. First, the material usually has a broad molecular weight distribution and a correspondingly large spread in the chain mobility. Second, the particles are often prepared by emulsion or miniemulsion polymerization and therefore carry a surfactant layer on the outside. The surfactant strongly influences the drying process.[14] Finally, the chemical composition often is spatially heterogeneous, where polar groups (such as acrylic-acid comonomers) tend to be located on the outside. Given these complications, it is important to have an experimental access to intermixing.

10.1021/ma800548r CCC: $40.75
Published on Web 06/21/2008

Data acquisition can proceed in different ways. A simple approach is based on the spectrum of the fluorescence, which changes as the fractional contributions from the donor and the acceptor decrease and increase, respectively. Basing the analysis on the fluorescence spectrum is not attractive for the studies pursued here because a turbid medium scatters blue light more efficiently than red light and thereby shifts the color toward the red. Since the samples investigated in this study are turbid, initially, and turn clear during the experiment, it is potentially misleading to base the analysis on color. Analyzing the decay curves from time-correlated single photon counting (TCSPC) is less prone to scattering artifacts. It suffices to consider the donor fluorescence alone. The decay curves of the donor, $I_D(t)$, contain the essential information. The analysis can either be based on the integral under the decay curve or on a fit of some suitable fit function to the decay curve. We mostly followed the latter procedure. We pay special attention to the final state of drying and therefore directly compare the respective decay curves to the predictions obtained with an analytical model and a simulation.

Traditionally, researchers have used FRET to monitor the progress of annealing after the film had become clear. This choice was partly motivated by experimental constraints. TCSPC requires pulsed light sources. Depending on the repetition rate and the intensity of the source, the speed of data acquisition can be a problem. The situation has much improved with the advent of UV-capable solid-state light emitting diodes (LEDs). These have repetition rates of up to 40 MHz at power levels around 1 μW. Using such a device, one can acquire decay curves at a rate of up to one data trace per minute. This increase in speed opens the way to apply FRET to films *while* they dry.

Experimental Section

We employed a light emitting diode ($\lambda_{max} = 282$ nm, PicoQuant, Germany) as the excitation source. Fluorescence photons were collected with a light guide in reflection mode. The detector was a photomultiplier tube (Hamamatsu 1P28). The correlation of the fluorescent photons with the pulses of the LED was carried out with modular electronics (ORTEC EG&G). We typically accumulated until the maximum number of counts per channel was 10^4. Two different filters were employed. The first filter (band pass, $\lambda = 325-480$ nm) cuts the excitation light well. Such a filter is a common choice in fluorescence experiments because scattering is considered an artifact to be avoided if ever possible. In contrast, the amount of scattering is a valuable piece of information when analyzing the drying of latex films. The disappearance of scattering marks the end of the compactification stage. We therefore also employed a second filter (cut-on, $\lambda_c = 320$ nm), which transmits part of the excitation light. By analyzing data traces acquired with this filter, we determined the scattering intensity and fluorescence decay curve, in parallel. Figure 1a shows data traces acquired with this filter. There is some excess signal coinciding with the lamp pulse, which originates from scattering. Only the first filter was employed in the FRET experiments because there is a rather significant amount of energy transfer in the first few nanoseconds. Scattering would have masked this essential part of the decay curve.

As the donor/acceptor pair, we used the monomers phenanthrene methacrylate (Phe−MA) and [1-(4-nitrophenyl)-2-pyrrolidinmethyl] acrylate (NPP−A).[15] Figure 2 displays the chemical structures. In the choice of the donor, we followed the Winnik group.[11] Phenanthrene is stable in free radical polymerization and has a low bleaching tendency. Its small size is an additional advantage. We chose NPP as the acceptor (rather than the more common anthracene) because it does not fluoresce itself and therefore does not interfere with the donor fluorescence. The Förster radius of the Phe−MA/NPP−A pair is $R_0 = 2.5$ nm.[15] NPP−A is available from Sigma-Aldrich, but we synthesized it on our own according to refs 16 and 17.

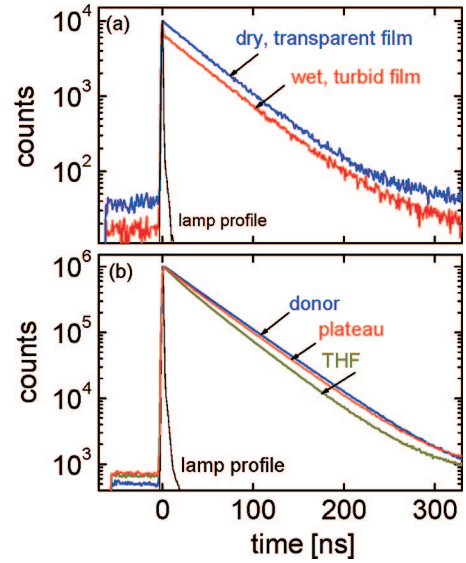

Figure 1. (a) Typical decay curves used for the kinetic analysis. Accumulation occurred until the maximum number of counts per channel was 10^4, corresponding to a data acquisition time between 1 and 3 min. These decay curves were acquired in the absence of the acceptor. The filter transmits some scattered excitation light. The bottom curve corresponds to a time immediately after spreading. There is a sizable number of excess counts in the first few channels, originating from scattering. The upper curve was taken on a clear film. The sharp peak coinciding with the lamp profile has disappeared. (b) Decay curves used for a detailed analysis of energy transfer in the plateau state (cf. Figure 6). Accumulation occurred until the maximum number of counts per channel was 10^6. The upper curve is the donor fluorescence in the absence of the acceptor. The center curve was acquired on a latex blend (1/1 donor/acceptor labeled) after drying at 30 °C. The bottom curve is from a sample where both the donor-labeled and the acceptor-labeled particles had been dissolved in THF, thereby producing a well-intermixed sample.

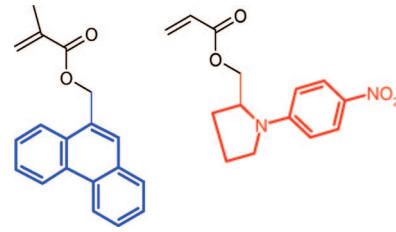

Figure 2. Chemical structure of the donor (phenanthrene methacrylate, Phe−MA, left) and the acceptor ([1-(4-nitrophenyl)-2-pyrrolidinmethyl] acrylate, NPP−A, right) in their monomeric form.

Table 1. Material Parameters

sample	composition [wt %] BA/MMA/AA	particle radius [nm]	M_w [g/mol] (M_w/M_n)	T_g [°C]	
L1	49/49/1	55	167 000 (3.6)	24	donor-labeled, 1 wt %
L2	49.4/49.4/1	65	116 000 (4.2)	23	acceptor-labeled, 0.2 wt %

We mostly report on copolymers of butyl acrylate (BA) and methyl methacrylate (MMA). Details of the materials are provided in Table 1. The particles were prepared by miniemulsion polymerization. The recipe was as follows: water (16 g), MMA (1.98 g), BA (1.98 g), acrylic acid (AA, 0.04 g), sodium dodecyl sulfate (SDS, 0.048 g), hexadecane (HD, 0.16 g), azobisisobutyronitril (AIBN, 0.068 g), and Phe−MA (0.0421 g, donor-labeled sample L1) or NPP−A (0.0084 g, acceptor-labeled sample L2) were placed in a small vial. Note that the initiator, AIBN, is uncharged. Chain ends are therefore not expected to be enriched at the particle surface. Water and organic phase were mixed for 3 min using a magnetic

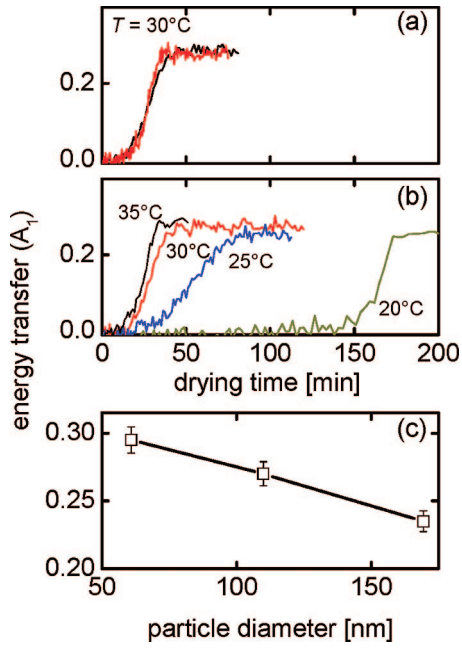

Figure 3. Panels a and b show the parameter A_1 (quantifying the efficiency of energy transfer) versus drying time. There is a step in kinetics of $A_1(t)$, associated with the formation of interparticle contacts. Key: (a) Results from two experiments carried out under identical conditions ($T = 30$ °C, humidity 40%rH). The kinetic curves are well reproducible. (b) Data acquired at slightly different temperatures. As expected, the speed of drying increases with drying temperature. (c) Values of A_1 reached in the plateau state versus particle size. The temperature was 30 °C in all cases. Smaller particles have a higher specific surface area and therefore contain a larger fraction of FRET-active donors.

stirrer at 2000 rpm. The mixture was sonicated (Branson sonifier 450, employing the microtip) for 30 min at 60% amplitude in the pulse-stop mode. The mixture was purged with nitrogen for 30 min and then heated to 70 °C. The reaction was kept at this temperature for 20 h and then cooled to room temperature. The conversion (determined gravimetrically) was between 98 and 99%. SEC (UV detection) traces taken from THF solutions of the resulting reaction mixtures do not show significant amounts of unreacted donor- or acceptor-monomer. The rather large amount of energy transfer discussed below can thus not be attributed to a fraction of highly mobile, low-molecular-weight species.

The glass temperature, T_g, of the polymer as determined with differential scanning calorimetry (DSC, Perkin-Elmer) was around 23 °C. The concentrations of the donor and the acceptor were 1.04 and 0.21 wt %, respectively. The molecular weights of the donor and the acceptor happen to be the same (276 g/mol), which leads to molar concentrations of 0.42 and 0.08 mol %, respectively. The concentration of the acceptor was chosen lower than the donor concentration for reasons of cost. Also, a small concentration of labels favors an even distribution of the label over the entire polymer phase. The choice of the monomer composition was motivated by the fact that similar recipes are widely used in the chemical industry. Including 1% of acrylic acid improves the colloidal stability. Generally speaking, the use of a copolymer entails the danger of compositional drift, possibly leading to phase separation and enrichment of the dye in one of the phases. We have checked for such effects in ref 15 with reference experiments on pure poly butylmethacrylate (p-BMA). The rates of energy transfer in this material and in the BA/MMA material (investigated in this study) were virtually the same, indicating that phase separation in the BA/MMA copolymer is not a problem.

The recipe given above produces particles with a diameter between 110 and 120 nm. We also show data obtained on smaller and larger particles in Figure 3c. These were obtained by increasing the amount of SDS to 0.28 g (smaller particles) or decreasing it to 0.0144 g (larger particles).

Particle sizes were determined by dynamic light scattering (DLS). The measurements were carried out at 25 °C on an ALV/DLS goniometer with a multi-τ digital correlator (5000E, ALV, Germany) at a scattering angle of 90°.

The films were formed on a glass plate. A mass of 60 mg was poured onto the plate and spread to an area of 1 cm^2 by means of a doctor blade. The wet thickness was around 600 μm. The setup was located inside a closed box. The temperature of the sample was controlled within ± 0.2 °C. Below, variable temperatures always pertain to the sample. The box was at room temperature. The humidity was 40 ± 3% rH. The film dried from the edge to the center, evidenced by the fact that the rim of the film became transparent first. The illuminated area was a round spot with an area of 3 mm^2. It was slightly displaced from the center of the film in order avoid effects related to the "very last drop".

Drying Kinetics. For every type of material and drying condition, we performed one experiment with a 1/1 mixture of donor-labeled and acceptor-labeled particles and a second experiment, where all particles were donor-labeled. The first type of material was used to determine the FRET efficiency, while the second one was used to measure the donor lifetime and the scattering intensity. In principle, it would of course be desirable to measure the scattering intensity, the donor lifetime, and the FRET efficiency all on the same sample. That would have entailed a substantial loss in the accuracy by which we determine the FRET efficiency and we therefore used separate samples with identical drying conditions. Since the experiments were well reproducible (Figure 3a, for the definition of the parameter A_1, quantifying energy transfer, see eq 2 below), we can compare the kinetics acquired on the two types of samples.

Varying the drying temperature in the range of room temperature (25−35 °C) does not change the picture much (Figure 3b). The height of the plateau slightly changes and the drying time decreases with increasing temperature. Figure 3c shows the value of A_1 on the plateau versus particle size. Smaller particles lead to a higher average FRET efficiency, which makes sense, considering that the specific surface area scales as the inverse particle radius.

Most measurements of the donor lifetime, τ_D, were carried out with a filter cutting the excitation light well. τ_D was determined by fitting the decay curves with a single exponential. Single exponentials produced reasonable fits when accumulating to a level of 10^4 counts per channel at maximum. More detailed investigations were carried out using a bandpass filter and accumulating to a level of 10^6 counts per channel at maximum. These revealed that the decay curves from the donor alone in fact were slightly nonexponential. We still use the results from fitting with a single exponential in the further analysis. Being precise, one might want to call the parameter τ_D "effective donor lifetime" because it is affected by of a variety of decay mechanisms not known in detail. We stick to the term "donor lifetime" for brevity.

In order to correlate donor lifetime and scattering intensity (that is, turbidity), we sometimes chose a filter which transmits some of the excitation light. These decay curves display in a sharp drop right after the excitation pulse and a monoexponential decay later on (Figure 1a, wet, turbid film). Unfortunately, this benefit comes at the expense of a sizable reduction in signal-to-noise ratio for the donor lifetime. We use the fit function

$$I_D(\tau') = \left\{ \tilde{A}_{sc}\delta(\tau') + I_0 \exp\left(-\frac{\tau'}{\tau_D}\right) \right\} \otimes I_{exc}(\tau') \qquad (1)$$

Here and in the following, τ' (in units of ns) is the time scale in the decay curves, whereas t (in units of minutes) is the drying time. $\delta(\tau')$ is the Dirac delta function. I_0 is a prefactor and $I_{exc}(\tau')$ is the lamp profile. $\tau_D(t)$ is the donor lifetime, which varies with drying time. $\delta(\tau')$ denotes convolution with the lamp profile. The excess signal coinciding with the excitation pulse is caused by scattering. We use the parameter $A_{sc} = \tilde{A}_{sc}/I_0$ as a measure of scattering intensity. Figure 4 shows results from two measurements, where scattering intensity and lifetime were acquired in parallel on the same sample. The scale of the

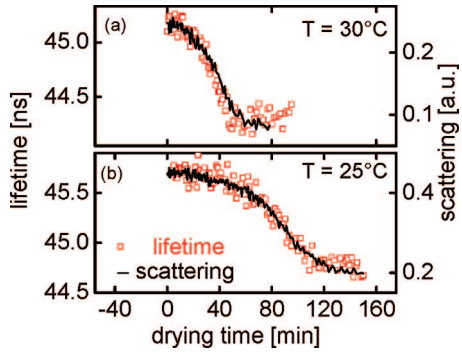

Figure 4. Plots of the lifetime and the scattering parameter versus drying time at two different temperatures. The scale of the scattering parameter, A_{sc}, was arranged such that the two data sets overlap. A_{sc} was derived from the excess signal in coincidence with the lamp profile (cf. Figure 1). These data were taken on samples containing no acceptor.

scattering intensity was chosen such that the two data traces overlap. Clearly, the kinetics is rather similar.

The fact that the kinetics of the scattering intensity and donor lifetime go in parallel suggests that the presence of water in the interstices has an effect on the lifetime. With regard to the influence of the environment on the fluorescence lifetime, two effects have to be distinguished.[18] The polarity of the environment affects the fluorescence properties on a rather short spatial scale. The refractive index (that is, the polarizability at optical frequencies) also is of influence, but this mechanism acts on a scale of at least the wavelength of light. The refractive index affects the spontaneous fluctuations of the electromagnetic field, which induce spontaneous emission when coupling to the dye. An increase in refractive index typically shortens the lifetime. We believe that the second mechanism underlies the observed decrease of donor lifetime with drying. In fact, we also observe a slight increase in donor lifetime upon thorough annealing at high temperatures (data not shown). Presumably, the latter increase goes back to a decrease of polarity in the immediate environment of the probe. Bulk water in the interstitial phase leads to scattering as well as a reduction in the refractive index, which explains our findings. Again, we associate both the drop in scattering intensity and in the donor lifetime to the disappearance of the interstitial phase.

The FRET efficiency was quantified by fitting the two-state model from ref 19 to the decay curves. Generally speaking, it is nontrivial to find a suitable fit function for decay curves acquired in the presence of acceptors. There is a distribution of distances and relative orientations, which translates into a distribution of lifetimes. There is no simple and, at the same time, realistic model which would lead to a fit function with easily interpreted fit parameters. For the purpose of kinetic analysis, we assume that there is some fraction of the donors, A_1, which is FRET-active, while the remaining fraction $(1 - A_1)$ is not. We use the fit function

$$I_D(\tau') = \left\{ A_1 \exp\left(-\frac{\tau'}{\tau_D} - 2\gamma\sqrt{\frac{\tau'}{\tau_D}}\right) + (1 - A_1)\exp\left(-\frac{\tau'}{\tau_D}\right)\right\} \otimes I_{exc}(\tau') \quad (2)$$

The parameter γ quantifies the concentration of acceptors around a FRET-active donor. A_1 is termed "FRET efficiency", in the following. In principle, one might use all four parameters of eq 2 (I_0, A_1, γ, and τ_D) as fit parameters. However, this leads to highly correlated errors. Of central importance in the kinetic analysis is transition between the initial state and the "plateau state", which is a stationary state reached during drying at room temperature (see Figure 3). In order identify the time of transition between these two states, it is more appropriate to fix γ and τ_D. We chose τ_D based on the plateau state of the sample in the absence of the acceptor. This section is not concerned with a detailed, quantitative interpretation of the value of A_1, but rather with the time of transition

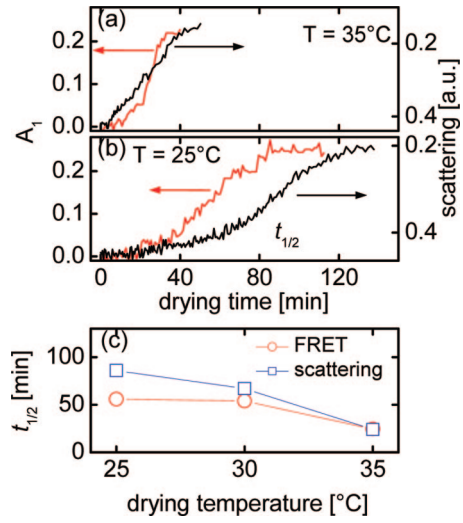

Figure 5. (a, b) Comparison of the kinetics of the FRET efficiency (thin line) and scattering efficiency (thick line) at two different temperatures. While the two kinetics are rather similar at $T = 35$ °C, the FRET efficiency goes through the transition earlier than the lifetime at $T = 25$ °C. The transition times, $t_{1/2}$, correspond to the times, where the respective parameters take values equal to the arithmetic averages of the values in the initial and the final state. Panel c displays the transition times, $t_{1/2}$, versus temperature.

between the initial state and the plateau state. The transition time, $t_{1/2,FRET}$ is unaffected by the choice of τ_D. A value of 0.45 was used for the parameter γ. This number was the outcome of an experiment, where films had been cast from THF.[15] For such films, intermixing should be perfect ($A_1 = 1$) and one can use γ (rather than A_1) as the free fit parameter. We have also tried to use the integral under the decay curve as an indicator of FRET-efficiency. The integral is derived in model-free way, which sounds attractive. However, the signal-to-noise ratio turned out to be inferior to the one reached with plots of $A_1(t)$.

In a first step, we elaborate on the time evolution of the FRET efficiency, the scattering intensity, and the donor lifetime. All three parameters display a sigmoidal dependence on drying time (Figures 3–5). Initially, the film is turbid, the donor lifetime is above 45 ns, and the FRET efficiency is below 0.03. At the end of drying, all three parameters are again constant. The film is largely transparent, the lifetime of the donor in the absence of the acceptor has decreased by about 1 ns, and A_1 has increased to 0.2−0.3. During high-temperature annealing, the scattering intensity further decreased, indicating the interstices had not yet collapsed completely in the plateau state. Note that the plateau state is not a thermodynamic equilibrium. Annealing increases the amount of polymer interdiffusion. We elaborate on annealing at the end of the Discussion.

Interestingly, the kinetics of the FRET efficiency, on the one hand, and the kinetics of the scattering intensity and the donor lifetime, on the other, do not always coincide. Figure 5c displays the times of transition between the initial state and the plateau state versus drying temperature. The two transition times agree for temperatures much above T_g. Around T_g, however, the formation of interparticle contacts precedes the disappearance of the interstitial phase. This is a result of appreciable practical relevance. The formation of hard coatings from polymer dispersions is a problem because hard polymer particles tend to either not deform at all, or to develop large stresses during the process of uniaxial compression. In the latter case, the spheres do deform, but film formation may still eventually fail because of cracking. If hard particles can be engineered such they develop cohesion shortly after they come into contact, this will help to prevent drying-induced fracture. We discuss the degree of intermixing attained after first contact in more detail in the next section.

FRET Efficiency in the Plateau State. Recalling that A_1 is the fraction of FRET-active molecules, a value of A_1 in the range of

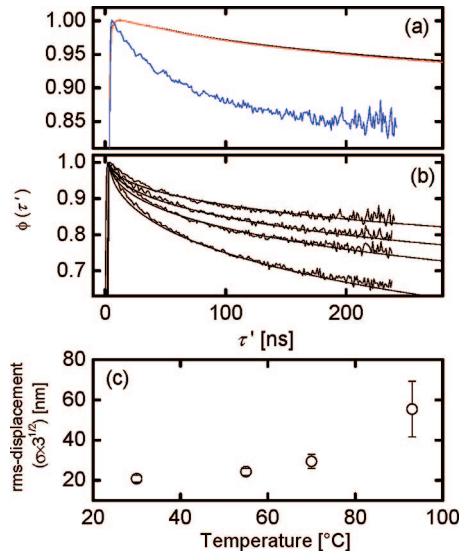

Figure 6. Comparison of the experimental decay curves with various predictions. The data have been divided by a convolution of $\exp(-\tau'/\tau_D)$ with the lamp profile for display purposes. The resulting function, $\phi(\tau')$, is the survival probability of a hypothetical donor molecule, which does not decay radiatively. (a) The two lines at the top (hardly distinguishable) are the predictions from an analytical model for a sharp interface (eqs 4 and 5) and the result of a simulation for the same situation. The experimental data set is the same as the one labeled with "plateau" in Figure 1b. It is incompatible with a sharp interface. (b) Experimental decay curves acquired on the plateau and simulation results, which match these curves. The drying temperatures were 30, 55, 70, and 93 °C (top to bottom). (c) Interface widths versus temperature as derived from the comparison of experiment and simulation. The *y*-axis shows the rms displacement of the dye molecules used in the simulations matching the experimental results best. It is about the same as the width of the interface.

0.2−0.3 reached for a dry (but otherwise untreated) film seems surprisingly high.

With a T_g around 20 °C, one would expect negligible polymer interdiffusion at room temperature. If FRET would occur across a sharp interface, a much lower value of A_1 would be expected. A value of A_1 in the range of 0.2 suggests that the range of intermixing is larger than a few molecular diameters.

In order to substantiate this argument, we first estimate the value A_1 expected for a sharp interface within the simple two-state model. The FRET-active donor molecules should be located in a shell at the border of the particle. The width of this layer should be about the Förster radius. Only 50% of these donors participate in energy transfer because only one-half of the neighboring spheres are labeled with acceptors, on average. Using a particle radius of $r_p = 55$ nm and a Förster radius of $R_0 = 2.5$ nm, one estimates A_1 as

$$A_1 \approx \frac{1}{2}\frac{V_{shell}}{V_{sphere}} = \frac{1}{2}\frac{4\pi {r_p}^2 R_0}{(4\pi/3){r_p}^3} = 0.07 \qquad (3)$$

This number clearly is below the experimental value of 0.2−0.3. On the other hand, choosing the width of the FRET-active shell as R_0 certainly is somewhat arbitrary. Also, the interface is distorted by compaction. We therefore also compare the decay curve acquired on the plateau to an analytical prediction and to a simulation (Figure 6a). The simulation also accounts for the distortion of the interface by compaction. With regard to the analytical treatment, we follow ref 20, where the latter assumes a sharp interface and a planar geometry. For clarity, the decay curves (both experimental and simulated) have been divided by a convolution of $\exp(-\tau'/\tau_D)$ with the lamp profile. This corrected curve shows the survival probability of a hypothetical excited donor molecule which does not directly fluoresce, ϕ.

The model from ref 20 has the donor lifetime, the Förster radius, and the thickness of the donor-labeled slab, *L*, as input parameters. It seems reasonable to apply this model to spheres (or more precisely, polyhedra) as long as the particle size much exceeds the Förster radius. The interparticle boundaries may then be modeled as planar. We chose the thickness of the equivalent planar slab, *L*, as equal to the sphere radius and accounted for the local curvature by including the normalized area of any given shell $(r_p - z)^2/{r_p}^2$ as a prefactor into the integrand. Here, *z* is the distance from the particle surface. The fact that only half of the surface is in contact with an acceptor-labeled particle is taken into account via an arithmetic average of the decay curve according to ref 20 and a simple exponential decay with lifetime τ_D. The following set of equations was used:

$$I_D(\tau') = \left\{ I_0 \exp\left(-\frac{\tau'}{\tau_D}\right)\left[\frac{1}{2} + \frac{1}{2}\int_0^{r_p} \frac{(r_p - z)^2}{{r_p}^2}\phi(z,\tau')\,dz\right]\right\} \otimes I_{exc}(\tau') \qquad (4)$$

$$\phi(z,\tau') = \exp\left\{-\frac{\pi}{3}C_A {R_0}^3 \sqrt{\frac{\tau'}{\tau_D}}\left\{2\Gamma\left(\frac{1}{2},T\right) - 3T^{-1/6}\Gamma\left(\frac{2}{3},T\right) + \frac{1-e^{-T}}{\sqrt{T}}\right\}\right\} \qquad (5)$$

$T = (\tau'/\tau_D)(R_0/z)^6$ is a normalized time and $\Gamma(\alpha,T) = \int_0^T u^{\alpha-1}e^{-u}\,du$ is the lower incomplete Γ-function. The integral in eq 4 requires numerical evaluation. We used the values $I_0 = 1$, $\tau_D = 45$ ns, $r_p = 55$ nm, $C_A = 0.02$ nm^{-3}, and $R_0 = 2.5$ nm. The two lines on the top of Figure 6a (hardly distinguishable) show the result of this calculation and the outcome of a simulation with a sharp interface (see below). The two lines agree well, but are at variance with the experiment.

Generally speaking, the shape of the decay curve reflects the concentration profile of donors and acceptors at the interface. Quantitative analysis is certainly possible. We are aware of two analytical approaches. The first is based on a mean-local-concentration model,[21] whereas the second one makes use of a Taylor expansion of $C_A(z)$ in the integrand.[22] Given the complexity of these equations and the assumptions needed, we preferred to do a simulation.[23] The simulation box of 450 × 450 × 450 nm contained a hexagonal array of particles. The interparticle distance was $2r_p \simeq 0.74^{1/3}$ where $r_p = 55$ nm is the sphere radius in the dispersed state as determined in dynamic light scattering and the factor of $0.74^{1/3}$ accounts for compaction. The interparticle distance is smaller than $2r_p$ because the particles have deformed. The simulation covers the situation *after* compaction. There is no interstitial phase. Also, the simulation does not contain a surfactant membrane separating the particles. Both an interstitial phase and a surfactant membrane would lower the FRET efficiency. The simulation therefore tends to overestimate the FRET efficiency or, equivalently, underestimate the degree of intermixing. The particles were randomly designated to be donor-labeled or acceptor-labeled. In a first step, fluorescent labels were randomly distributed inside the simulation box. This procedure generated a distribution of labels corresponding to ideally flat interfaces. In a second step, all labels were displaced from their original positions by some vector $\Delta\boldsymbol{r}$. The direction of displacement was random and the length of the vector was distributed as a Gaussian with width σ. The mean-square displacement of the donors is $3\sigma^2$. Figure 7 shows a snapshot.

For Fickian diffusion, the parameter σ would equal $2Dt$. For $\sigma \ll r_p$, the width of the intermixed boundary layer is about 2σ. We discarded strips of width 2σ at the edges of the simulation box from the analysis in order to avoid artifacts related to the finite size of the box. The simulation results shown in Figure 6b are averages over 10 runs. Some simulations were run in the presence of a small fraction of monomeric, highly mobile labels (1%). These where randomly redistributed in the entire box during the diffusion step. At a level of 1%, the mobile fraction did not significantly change the modeling results.

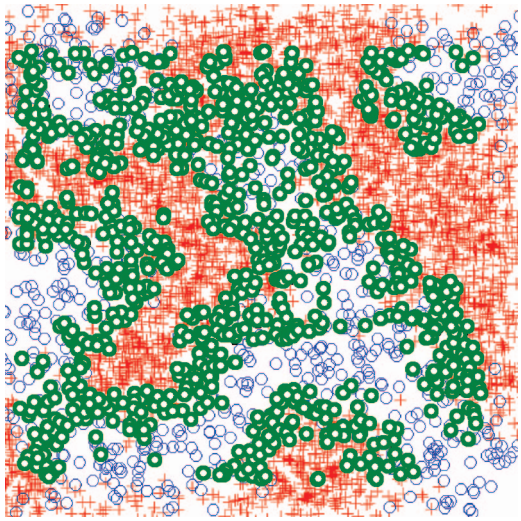

Figure 7. Cross section of the simulation box, showing the distributions of labels. Crosses and thin open dots are donors and acceptors, respectively. Thick open dots mark donors, the lifetime of which is less than 0.98 τ_D. The thickness of the cross section is 2 nm. The rms displacement was 26 nm.

Decay curves were generated with the following equations:

$$I_{\mathrm{D}}(\tau') = \left\{ \frac{1}{n_{\mathrm{don}}} \sum_{i=1}^{n_{\mathrm{don}}} \exp\left(-\frac{\tau'}{\tau_i}\right) \right\} \otimes I_{\mathrm{exc}}(\tau')$$

$$\tau_i^{-1} = \tau_{\mathrm{D}}^{-1} \left(1 + \sum_{j=1}^{n_{\mathrm{acc}}} \left(\frac{R_0}{r_{ij}}\right)^6\right) \qquad (6)$$

The indices i and j run over the donor and acceptor molecules, respectively. r_{ij} is the intermolecular distance and R_0 is the Förster radius. For sharp interfaces, the simulation result comes close to the analytical result (eq 4 and eq 5, top in Figure 6a).

Figure 6b shows a number of experimental decay curves together with simulation results matching the experimental data. These experimental decay curves (accumulation to 10^6 counts at peak, data acquisition time $\sim$ 90 min) were taken after quenching the dried sample (drying time of 60 min) to room temperature. In the case of drying at 93 °C, the plateau actually was slightly sloped (cf. Figure 8a). The quench to room temperature was needed because the donor lifetime slightly depended on temperature. In order to compare the different decay curves shown in Figure 6b, the temperature during data acquisition must be the same for all data sets. As expected, the degree of intermixing depends on the drying temperature.

Figure 6c shows the interface width derived by comparing experiment and simulation. For the sake of comparison, we plotted simulated and experimental decay curves in the same graph (panel b) and varied the interface width used in the simulation (or, more precisely, the rms displacement) until the simulated decay curve matched the experimental one. Whether or not a good "match" had been achieved was judged by eye. The same applies to the error bars on the derived interface widths. Again, the derived interface widths may be considered as lower bounds because the simulation ignores the presence of the surfactant. The temperature dependence of the rms-displacement actually is rather moderate for temperatures of up to 70 °C (given that viscosity changes by orders of magnitude between 30 and 70 °C). Only at 93 °C does one find a strongly increased value for σ. This finding suggests that the width of intermixed layer below 70 °C is not governed by the material's viscosity, but by some other system parameter (such as R_g or the entanglement length, see end of Discussion).

Annealing Experiments. Rather than following diffusive behavior, the FRET efficiency levels off during drying and ends in a plateau state. This raises the question of whether or not these films behave diffusively in thermal annealing. Results from annealing experiments are shown in Figure 8b. For films which have been dried at 30 °C, a temperature jump to 93 °C is instantaneously followed by a jump in A_1. The jump is much too large to be attributed to a temperature-dependent lifetime. Keeping the sample at 93 °C, one observes the familiar further increase of A_1, which is caused by conventional interdiffusion.

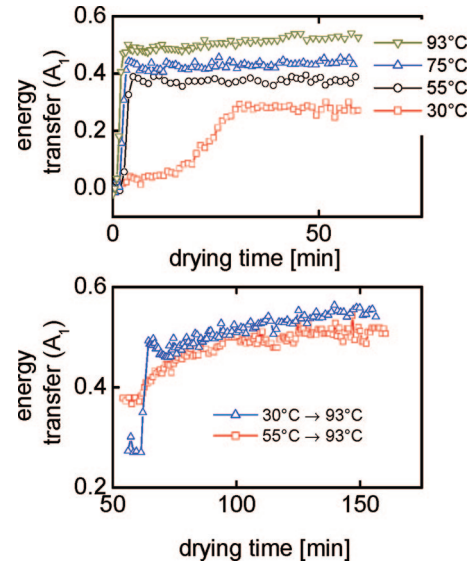

Figure 8. (a) Drying at elevated temperatures leads to a plateau in FRET efficiency. Only the sample dried at 93 °C shows some further interdiffusion after the plateau has been reached. (b) Annealing experiments. Samples dried at 30 °C show a jump in FRET efficiency upon jumping the temperature, whereas no such jump is seen for films dried at 55 °C.

Drying the sample in vacuum overnight did *not* change the magnitude of the jump. Note, however, that vacuum drying will presumably only remove interstitial water. Water tightly attached to surfactant or to acrylic acid groups is not expected to be removed under vacuum.[24] Interestingly, the jump *was* removed by drying the samples at 55 °C (and afterward jumping the temperature to 93 °C). Drying at 55 °C changes the state of a film a way which is substantially different from drying at room temperature in vacuum. The drying temperature is more important for the physical properties of the plateau state than the environmental humidity.

Discussion

On the basis of the evolution of FRET efficiency with time, we conclude that a well-intermixed layer with a width of at least 20 nm develops at the interparticle junctions soon after the particles come into contact. However, intermixing comes to halt after this layer has developed. Further interdiffusion can only be brought about by thermal annealing.

The plateau in the FRET efficiency clearly evidences the existence of a soft shell (a "liquidlike layer") at the particle surface. With regard to its molecular origin, two explanations come to mind. First, the shell might be more hydrophilic than the bulk, leading to preferential plasticization.[25] The dispersion contains a hydrophilic comonomer. In order to match the practice widely adopted in industry, we added 1% of acrylic acid (AA) to the monomer base. The acrylic acid component is commonly believed to be enriched at the particle surface,[26] which improves the colloid stability. The second hypothesis builds on geometric confinement. Anomalous softness of glassy materials close to interfaces has been in much detail investigated in the recent years.[27,28] Landfester and Herminghaus have shown that similar soft shells also exist for polystyrene particles prepared by miniemulsion.[29,30] These authors attribute the softness to confinement.

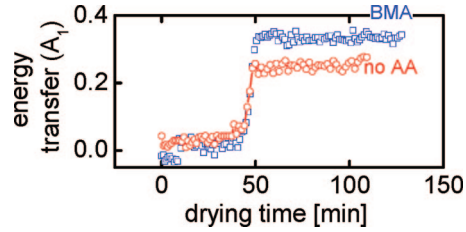

Figure 9. Reference experiments on a sample containing no acrylic acid (open circles) and on a homopolymer of *p*-butyl methacrylate (BMA, open squares). The results closely resemble the results shown in Figure 3. The liquidlike layer can neither be attributed to the presence of acrylic acid, nor to internal phase separation between BA and MMA.

In order to further investigate the mechanism underlying the formation of the liquidlike layer, we have performed two experiments where we varied the chemical composition of the particles. First, we studied films made from a material containing no acrylic acid. These dispersions showed poor colloid stability, but films could be formed soon after polymerization, nevertheless. As Figure 9 shows, a plateau develops for this sample in the same way as for samples which do contain AA. Clearly, the liquid-like layer cannot be attributed to an AA-enriched shell. The second check concerns the possibility of compositional drift and phase separation inside the polymer particles. The copolymerization parameters are such that material produced at late times may be enriched in BA and might also—in principle—phase-separate from the material produced at earlier times. The soft shell might be composed of BA-enriched material and therefore be softer than the bulk. However, spheres composed of the homopolymer poly butylmethacrylate (BMA) show essentially the same behavior as the copolymer, excluding phase separation as the likely explanation (Figure 9). Without having detailed experimental proof, we also note that enrichment of short chains at the particles surface is unexpected. This effect is known from conventional emulsion polymerization, where the initiator enters from the outside.[31] Chains growing at the edge of the particle are, on average, terminated earlier than chains growing in the center. However, this study made use of miniemulsion polymerization, where this effect is absent.

We performed some experiments in order to address the question of whether the liquidlike layer is mostly caused by plasticization by water or rather by confinement. Films were formed at 30 °C and then dried under vacuum overnight (Figure 8). Upon annealing at 93 °C, the moist films (not dried in vacuum) and the vacuum-dried films both show jumps in A_1. The magnitudes are about the same. Assuming that the vacuum-dried films contain less water, this result speaks in favor of the confinement hypothesis. Note, however, that tightly bound water may have remained inside the film despite the vacuum treatment.

Within the soft-shell picture, the jump in A_1 is explained as an increase in the effective width of the soft layer. Presumably, the soft layer does not have a discrete boundary, but should rather be described as a gradient in softness. At any given temperature, interdiffusion happens in those parts of the particle where the local T_g is below the drying temperature. Increasing the drying temperatures therefore effectively widens the "soft layer". Interestingly, no further jump in A_1 is observed when annealing a sample which was initially dried at 55 °C. The interdiffusion actually proceeds *slower* than in the case of films dried at 30 °C. Evidently, drying at 55 °C partially removes the liquidlike layer. It renders the near-surface material more bulk-like.

The width of the intermixed layer as shown in Figure 6c is starkly at variance with the expectations from standard polymer dynamics, as the following estimate shows. We derive an upper limit for the rms-displacement expected for bulk-like diffusion. Assume that the chains behave Rouse-like. The observed rms-displacement ($3^{1/2} \times \sigma \sim 20$ nm) is somewhat above the typical tube diameter usually assumed in reptation theory (a few nm), but the surfactant may have enlarged the tubes. Assume that the diffusion coefficient obeys $D_{chain} = k_B T/(\zeta N)$ with ζ the monomer friction coefficient and $N \sim 1000$ the number of segments. ζ can be approximated as $\zeta \sim 6\pi\eta r_H$ with η the viscosity and r_H the segmental radius. The viscosity should be somewhere in the range of 10^{10} Pa s for a material close to T_g. At T_g, η is around 10^{12} Pa s. The segmental radius is around 0.3 nm. This estimate leads to $D_{chain} \sim 3 \times 10^{-22}$ cm^2/s. With a diffusion time of one hour, we arrive at an rms-displacement of 0.01 nm. This value is three decades below the experimental rms-displacement of about 20 nm. The estimate above concerned a chain with a length equal to the number-average and, also, it concerned diffusion of entire chains (as opposed to segmental motion). However, given that the rms displacement scales as the $N^{-1/2}$, it is impossible to bridge a gap of three decades by attributing the diffusion to a mobile fraction of short chains.[32] Segmental diffusion can also not explain an rms displacement of 20 nm because the radius of gyration of the chains is only about 10 nm.

Conclusions

We have studied the drying of latex dispersions based on the efficiency of energy transfer between donor and acceptor molecules, the scattering intensity, and the lifetime of the donor molecules. All three parameters vary sigmoidally with drying time. The kinetics of the donor lifetime closely correlates with the kinetics of the scattering intensity. The shifts in scattering intensity and donor lifetime mark the disappearance of the interstitial phase. Interparticle cohesion as reflected by the FRET efficiency frequently develops *before* the interstitial phase disappears. These findings prove that neighboring polymer spheres develop an intermixed layer immediately after they come into contact. Comparing the experimental data with computer simulations, we conclude that the width of the intermixed layer was at least 20 nm, depending on the drying temperature. Presumably, interdiffusion is aided by a liquidlike layer. The effect does not rely on a hydrophilic shell and it is not caused by nanoscale phase separation. The formation of a cohesive contact during the particle deformation stage should help to prevent cracking.

Acknowledgment. This work was funded by the EU under Contract IP 011844-2 (NAPOLEON). The material NPP-A was kindly provided by Dr. Irina Martynova.

References and Notes

(1) Keddie, J. L. *Mater. Sci. Eng. R-Rep.* **1997**, *21*, 101.
(2) Steward, P. A.; Hearn, J.; Wilkinson, M. C. *Adv. Colloid Interface Sci.* **2000**, *86*, 195.
(3) Winnik, M. A. *Curr. Opin. Colloid Interface Sci.* **1997**, *2*, 192.
(4) Dillon, R. E.; Bradford, E. B.; Andrews, R. D. *Ind. Eng. Chem.* **1953**, *45*, 728.
(5) Voyutskii, S. S. *J. Polym. Sci.* **1958**, *32*, 528.
(6) Perez, E.; Lang, J. *Langmuir* **2000**, *16*, 1874.
(7) Sambasivam, M.; Klein, A.; Sperling, L. H. *J. Appl. Polym. Sci.* **1995**, *58*, 357.
(8) Hahn, K.; Ley, G.; Schuller, H.; Oberthur, R. *Colloid Polym. Sci.* **1986**, *264*, 1092.
(9) Kim, S. D.; Klein, A.; Sperling, L. H. *Polym. Adv. Technol.* **2002**, *13*, 403.
(10) Linne, M. A.; Klein, A.; Sperling, L. H.; Wignall, G. D. *J. Macromol. Sci.: Phys. B* **1988**, *27*, 181.
(11) Zhao, C. L.; Wang, Y. C.; Hruska, Z.; Winnik, M. A. *Macromolecules* **1990**, *23*, 4082.
(12) Pekcan, O.; Winnik, M. A.; Croucher, M. D. *Macromolecules* **1990**, *23*, 2673.

(13) Liu, Y. Q.; Haley, J. C.; Deng, K.; Lau, W.; Winnik, M. A. *Macromolecules* **2007**, *40*, 6422.
(14) Kientz, E.; Holl, Y. *Colloids Surf. A* **1993**, *78*, 255.
(15) Turshatov, A.; Adams, J. *Polymer* **2007**, *48*, 7444.
(16) Zyss, J.; Nicoud, J. F.; Coquillay, M. *J. Chem. Phys.* **1984**, *81*, 4160.
(17) Iftime, G.; Natansohn, A.; Rochon, P. *Macromolecules* **2002**, *35*, 365.
(18) Toptygin, D. *J. Fluorescence* **2003**, *13*, 201.
(19) Wang, Y. C.; Zhao, C. L.; Winnik, M. A. *J. Chem. Phys.* **1991**, *95*, 2143.
(20) Yekta, A.; Duhamel, J. Winnik, M.A.;. *Chem. Phys. Lett.* **1995**, *235*, 119.
(21) Dhinojwala, A.; Torkelson, J. M. *Macromolecules* **1994**, *27*, 4817.
(22) Farinha, J. P. S.; Martinho, J. M. G.; Yekta, A.; Winnik, M. A. *Macromolecules* **1995**, *28*, 6084.
(23) Haley, J. C.; Liu, Y.; Winnik, M. A.; Demmer, D.; Haslett, T.; Lau, W. *Rev. Sci. Instrum.* **2007**, *78*, 084101.
(24) Rottstegge, J.; Traub, B.; Wilhelm, M.; Landfester, K.; Heldmann, C.; Spiess, H. W. *Macromol. Chem. Phys.* **2003**, *204*, 787.
(25) Sperry, P. R.; Snyder, B. S.; Odowd, M. L. Lesko, P.M. *Langmuir* **1994**, *10*, 2619.
(26) Chevalier, Y.; Pichot, C.; Graillat, C.; Joanicot, C.; Wong, K.; Maquet, J.; Lindner, P.; Cabane, B. *Colloid Polym. Sci.* **1992**, *270*, 806.
(27) Alcoutlabi, M.; McKenna, G. B. *J. Phys.: Condens. Matter* **2005**, *17*, R461.
(28) Priestley, R. D.; Ellison, C. J.; Broadbelt, L. J.; Torkelson, J. M. *Science* **2005**, *309*, 456.
(29) Seemann, R.; Jacobs, K.; Landfester, K.; Herminghaus, S. *J. Polym. Sci., Part B* **2006**, *44*, 2968.
(30) Herminghaus, S.; Seemann, R.; Landfester, K. *Phys. Rev. Lett.* **2004**, *93*, 017801.
(31) Thickett, S. C.; Gilbert, R. G. *Polymer* **2007**, *48*, 6965.
(32) Veniaminov, A.; Jahr, T.; Sillescu, H.; Bartsch, E. *Macromolecules* **2002**, *35*, 808.

MA800548R